Laboratory spectral induced polarisation signatures associated with iron and manganese oxide dissolution because of anaerobic degradation.

Perrine M. Fernandez[1], Andrew Binley[2], Esther Bloem[3] and Helen K. French[1,3]

[1]Norwegian University of Life Sciences (NMBU), Universitetstunet 3, 1430 Ås, Norway

[2]Lancaster Environment Centre, Lancaster University, Lancaster LA1 4YQ, United Kingdom

[3]Norwegian Institute of Bioeconomy Research (NIBIO), Høgskoleveien 7, 1430 Ås, Norway

Corresponding author: perrine.m.fernandez@gmail.com

Emails of the authors: perrine.m.fernandez@gmail.com, a.binley@lancaster.ac.uk,

Esther.Bloem@nibio.no, helen.french@nmbu.no

Abstract. Degradation of organic chemicals in natural soils depends on oxidation-reduction conditions. To protect our groundwater resources we need to understand the degradation processes under anaerobic conditions. Available iron and manganese oxides are used as electron acceptors for anaerobic degradation and are reduced to the dissolved form of metallic cations in pore water. To monitor this process is a challenge, because anaerobic conditions are difficult to sample directly without introducing oxygen. A few studies have shown an impact of iron reduction on spectral induced polarisation (SIP) signature, often associated with bacterial growth. Our objective is to study the impact of iron and manganese oxide dissolution, caused by degradation of an organic compound, with spectral induced polarisation signatures.

Twenty-six vertical columns (30cm high, inner diameter 4.6cm) were filled with a sand rich in oxides (manganese and iron) with a static water table in the middle. In half of the columns, a 2cm high contaminated layer was installed just above the water table. As the contaminant degrades, the initial oxygen is consumed and anaerobic conditions form Every three days over a period of one month, spectral induced polarisation (twenty frequencies between 5mHz and 10kHz) data were collected on six columns: three contaminated replicates and three control replicates. Chemical analysis was done on twenty columns assigned for destructive water sampling, ten contaminated columns and ten control.

The results show an increase of the real conductivity associated with the degradation processes, independent of frequency. Compared with the pore water electrical conductivity in the saturated zone, the real conductivity measurement revealed the formation of surface conductivity before iron was released in the pore water. In parallel, we also observed an evolution of the imaginary conductivity in both saturated and unsaturated zones at frequencies below 1Hz. Overall, the anaerobic reduction of iron and manganese oxide during the organic degradation increased both the conductive and polarisation component of the complex conductivity.

Highlights.

- σ' increase is frequency independent when metallic ions are released in pore water
- σ'' increases around 0.1Hz before metallic ions are released in pore water
- Mineralogical changes preceding the ion formation probably explained σ'' trend
- Results were reproduced in triplicates and compared with controls

1. Introduction

Mapping the redox situation in soils is relevant for many applications including agriculture, especially in saturated soils such as rice paddies, the release of climate gases from peat systems; for the protection of buried organic cultural heritage and wooden building foundation materials, with the aim to reduce degradation by preserving anaerobic conditions; for landfill and contaminated site management. Examples of in-situ preservation monitoring in unsaturated cultural layers in Norway are found in the medieval towns of Trondheim (Petersén and Bergersen, 2012 and 2016) and Oslo (Martens et al., 2012). Examples showing the importance of anaerobic conditions in the unsaturated zone include those monitoring the fate of de-icing chemicals in airport soils (French et al., 1999; Nitschke et al., 1996; Jaesche et al., 2006; Murphy et al., 2015). Whether the goal is to protect historical remains or the groundwater quality, identifying the degradation conditions is important, but challenging since redox reactions seldom are at equilibrium in groundwater (Lindberg and Runnells, 1984) and obtaining reliable measurements is difficult. The major problem with destructive sampling is that oxygen becomes available while drilling or digging the sample, which immediately changes the redox conditions. Traditional in situ measurements of redox potential (E_h) with a platinum electrode and a reference electrode can be difficult to perform (Nyquist and Corry, 2002), because most probes (like combined Oxidation-Reduction Probes, ORP) are designed for water, not soil measurements (Fernandez et al., 2015). Furthermore, these measurement techniques only provide point measurements and thus are limited in heterogeneous environments. Therefore there is a need for non-intrusive methods to characterise redox conditions. Recently, various studies used geophysical methods successfully for environmental monitoring involving redox degradation, for example self-potential signal (e.g. Arora et al., 2007), 3D electrical resistivity imaging (e.g. Maurya et al., 2017) and induced polarisation (e.g. Balbarini et al., 2018). Still, more study are needed to link complex redox processes to their geophysical signatures.

Induced polarisation (IP) is a century old electrical geophysical method developed by Schlumberger (1920) which is sensitive to both conductive and polarisation properties of the subsurface. The IP signature is a complex conductivity, with conductive property expressed in the real part and the polarisation properties express in the imaginary part. Since the mid-20th century, IP has been used extensively in geological exploration for ores and hydrocarbons. Recently, IP has also been applied to characterise soil contamination (e.g. Carlson et al., 2015; Maurya et al., 2017). While the electrical resistivity technique measures the stabilised electrical

potential in the ground during injection of current, IP measures the transient voltage after the current is switched off. The composition of the soil system, for example mineralogy, microbial community and fluid composition, have an influence on the polarisation, and the decay time reflects these properties. The polarisation of the ground can respond differently to the frequency of the injected current cycle, this has given rise to spectral induced polarisation (SIP).

Our hypothesis is that, in the context of redox degradation, SIP is sensitive to the anaerobic dissolution of iron and manganese oxides. Anaerobic degradation can lead to manganese and iron reduction and release of sulphide (e.g. Appelo and Postma, 2010). That the increased complex conductivity associated with sulphide release can be measured with spectral induced polarisation is well documented (eg. Williams et al., 2009; Placencia-Gomez et al., 2013). Williams et al. (2009) also observed a phase angle increase with the use of frequencies in the range of 1-50Hz caused by iron reduction, though not as pronounced as what was observed for sulphide release. Ntarlagiannis et al. (2005) associated polarisation anomalies with metal reduction and higher microbial population. Abdel Aal et al. (2010) showed that bacterial growth in iron oxide coated sand increased the imaginary conductivity by 30-40% compared to clean quartz sand. Although there have been some applications of SIP monitoring of iron oxide dissolution, manganese oxide dissolution remains largely unexplored.

This paper examines changes in SIP signals caused by the development of reducing conditions during degradation of an organic contaminant at the water table interface. The hypotheses is that the development of reducing conditions with dissolution of iron and manganese will increase the complex conductivity, similarly to what Williams et al. (2009) observed for iron dissolution. In this study, propylene glycol, a common de-icing chemical, was used as a degradable carbon source in a soil known to release high concentrations of iron and manganese (French et al., 2001; Lissner et al., 2013, Fernandez et al., 2018). The study was conducted in a set of twenty-six sand columns under static water conditions. Replicated samples of each of the treatments were set up for the SIP measurements, which is noticeably uncommon in previous related geophysical studies.

2. Material and Methods

Twenty-six columns under static hydraulic conditions were setup in the laboratory. They were filled with sand and a stable water table half way up the column. The sand was collected and mixed from the top 1 m of a glaciofluvial deposit, at Moreppen, near Oslo airport (location

described in French et al., 2001; French and Binley, 2004). A solution of propylene glycol (PG) and a conservative chemical tracer (LiCl) was added just above the established water table in 13 of the columns (hereafter called *contaminated columns*). In order to compare the effect of PG degradation with background conditions (same geology, temperature, depth), the other 13 columns only contained reference water (hereafter called *control columns*). Indirect and direct methods were used to monitor the changes caused by degradation and dispersion:

1) Time-lapse spectral induced polarisation (indirect method) to follow the changes in conductivity and polarisation.
2) Water samples (direct method) to monitor changes in pore fluid chemistry.

2.1. Column setup

The PVC columns, 4.6cm diameter and 30cm long, sealed at both ends with plastic caps, were considered one dimensional and the reference point (Z=0) was given at the bottom of the column as indicated in Figure 1. Since this was a static system, water could not be sampled without changing the water content and create a risk of disturbing the redox conditions by providing additional oxygen. Hence, at each time step, one column was used for destructive sampling of pore water. During the 36 day period of the experiment, ten contaminated columns and ten control columns were used for this purpose. The other six columns (three contaminated and three control) were used as replicates for time-lapse SIP measurements. For the SIP columns, the initial SIP measurement started on day 3 after the contaminant placement had taken place; these were repeated every three days. On the SIP measurement days pore water sampling was done in one of the contaminated and control destructive columns, which started on day 6. Figure 1 shows a sketch of the different types of columns with their important elements: water table, PG and lithium (LiCl) tracer location, electrodes and sample locations. Six PVC access pipes (0.5cm I.D, 2cm long) separated by 4cm were installed perpendicular to the SIP columns. The lowest one (at Z=6cm) controls the water table. The potential electrodes A, B, C, D, E (Figure 1) are placed in the five others access pipes (Z_E=10cm, Z_D=14cm, Z_C=18cm, Z_B=22cm, Z_A=26cm). The column caps at both ends of the columns were pierced for installation of the current electrodes; the holes were sealed with silicon once the electrodes were in place to prevent moisture loss.

All the columns were initially filled with a predefined solution of 2mmol/L NaCl dissolved in 100mL deionised water to make the water conductive (EC=210µS/cm, pH 4.9). The columns were completely filled with Moreppen sand (sieved <2mm, 99.3% sand, 0.7%

silt-clay fraction, 1.8% organic matter), naturally rich in manganese (0.7g/kg) and iron (20g/kg), to a porosity of 41%. The sand was sprinkled carefully from the top of the column to avoid trapping air. To estimate evaporation, two columns, identical to the rest of the batch, were weighed regularly for two weeks prior to the main experiment. These showed an evaporation rate of 10mg/day per column. For an initial water volume of 100mL, this represents 0.42% total loss of water mass throughout the experiment. The water level remained constant in all the SIP columns. The water table was set at Z_{WT}=18cm in all the columns, but the remaining 12cm above had a relatively high water content due to the large capillary fringe.

2.2. PG contamination

To make the location of the PG addition as a precise and confined as possible (to obtain 1D conditions), 33cm^3 batches of sand were soaked (saturation 0.75) with a solution of NaCl (0.12g/L), PG (90g/L) and lithium tracer LiCl (1g/L), with EC=1570μS/cm and placed as 2cm thick layer in the column during construction of the columns. The contaminated sand was placed between Z=18cm and Z=20cm in the thirteen contaminated columns. With a very low clay content (silt and clay represent 0.7% of the material), lithium sorption was considered negligible and therefore a conservative chemical tracer. Both PG and lithium concentrations were expected to decrease over time due to dilution, and in addition degradation of PG.

2.3. Spectral induced polarisation

Induced polarisation measurements are made with two potential electrodes after injecting current between two other electrodes. Five non-polarisable potential electrodes were installed in each of the six columns for SIP measurements. The electrodes were silver coated in silver chloride (In Vivo Metric, California) and mounted in a rubber cork on a needle wrapped in PTFE film. The cork was pushed into the access pipes of the column (Figure 1) until the electrode was in good contact with the sand. In each of the six columns, two current electrodes made of stainless steel mesh covered the surface of the caps at both ends of the column (Z=0cm and Z=30cm). The current electrodes were extended through the caps and out of the columns with a copper wire.

To monitor changes in polarisability, SIP measurements were performed every 3 days for both sets of columns: with and without PG. For each replicate, the data were collected between three pairs of potential electrodes: pair AB (unsaturated zone), BC (unsaturated zone, just above the water table, initial location of PG) and DE (saturated zone) (Figure 1). Each location was measured for 22 frequencies ranging from 5mHz to 45 kHz (5mHz, 10mHz,

30mHz, 50mHz, 100mHz, 200mHz, 500mHz, 1Hz, 2Hz, 5Hz, 10Hz, 30Hz, 70Hz, 130Hz, 200Hz, 500Hz, 1kHz, 2kHz, 4kHz, 10kHz, 20kHz and 45 kHz). This covers the range 100mHz-1kHz used to detect hydrocarbon biodegradation (Abdel Aal et al., 2006) and iron precipitation (Slater et al., 2005; Placencia-Gómez et al., 2013). The amplifier was a SIP-System ZEL-SIP04-V05 (from Forschungszentrum Jülich) and the function generator an Agilent 33220A. Due to errors in one of the water column replicates, data from only two replicates are reported. Data from all three replicates are shown for the contaminated columns.

For a given frequency, the soil responds to an alternating current in two ways: an in-phase component (the real conductivity) and an out-of-phase component (quadrature or imaginary conductivity), the latter being a measure of the polarisation of the soil. The quadrature conductivity is inferred from a measured phase shift between injected current and measured voltage. As explained in more detail by Kemna et al. (2004), SIP can be characterised by the complex conductivity, σ^{*}:

$$\sigma^{*} = \sigma' + i\sigma'' \tag{1}$$

with σ' the real conductivity, σ'' the imaginary conductivity and i the imaginary unit defined by $i^2 = -1$. We used spectral induced polarisation to look for irregularities in the real and imaginary conductivity for a range of frequencies, and their variation in time at a given frequency.

The measured real conductivity comes from the surface conductivity, which is the conductivity along the grain boundaries and the pore water conductivity. By using Archie's law on the pore water conductivity in the saturated zone, the surface conductivity can be expressed as:

$$\sigma'_{surface} = \sigma'_{total} - \sigma_{fluid} \cdot \phi^{m} \tag{2}$$

where $\sigma'_{surface}$ is the contribution of surface conductivity, σ'_{total} the measured bulk conductivity, σ_{fluid} is the measured electrical conductivity of the pore water samples, ϕ the porosity, measured to be 0.41 and assumed constant, and *m* the cementation factor of 1.9 calculated for this Moreppen sand (Søiland, 2011).

2.4. Water analysis

Pore-water was sampled every three days starting on day 6. Each time pore water samples were needed, a contaminated column and a reference column were sampled and

destroyed. To limit oxygen exposure while sampling pore water, Rhizon Flex (Rhizoshphere, 10cm long, o.d. 0.25cm) were used at two locations in each of the destructively sampled columns. On the sampling da y, two holes were drilled: one above (Z=20cm, unsaturated zone) and one below (Z=11cm, saturated zone) the initial PG release location (Figure 1). With a mean pore diameter of 0.15µm of the Rhizon Flex, the extracted water was free of particles. Water samples were extracted by attaching the PVC tubing from the filters to a 50mL evacuated syringe. The water sampler did not contain any metal parts to avoid contamination. The samples (15mL per location) were analysed for pH, EC, PG, iron, manganese and lithium. The 2mL samples required for PG analysis were stored frozen until analysed using Schotten-Bauman method of benzoylation of glycols (Perkin-Elmer HPLC UV/Vis detector, with limit of quantification 0.1mg/L). Water samples were analysed according to standards on an Inductively Coupled Plasma Optical Emission Spectrometry (ICP-OES) for iron, manganese and lithium.
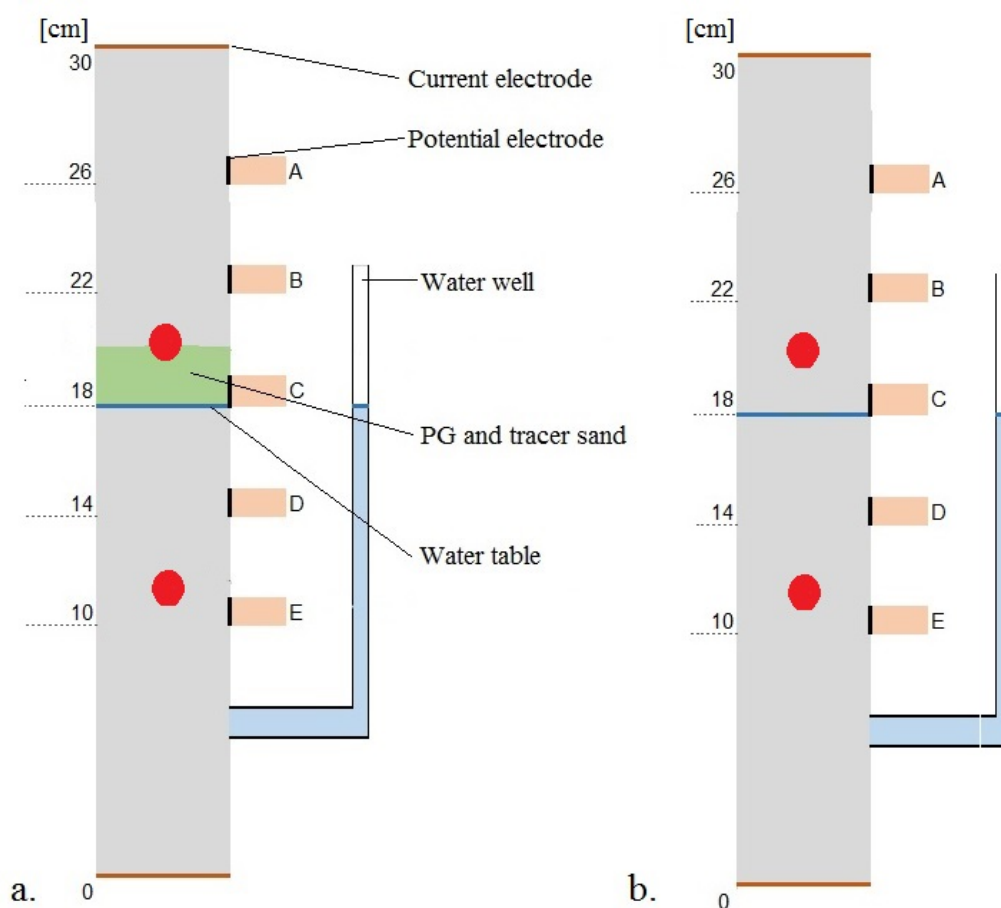

Figure 1. Column setups for SIP measurements **a.** with PG and lithium tracer (contaminated column) and **b.** control column. The water table is marked as a blue line. The green area shows the location of the sand layer contaminated with PG and lithium tracer. The red dots show water

sampling locations in the destructive columns. Locations A-E show positions of the potential electrodes, the current electrodes are located at both ends (in brown).

3. Results

3.1. Real conductivity (SIP)

The measured real conductivity was independent of frequency between 5mHz and 10kHz. The standard deviation of the real conductivities based on 20 frequencies was on average 0.3mS/m. In the saturated zone (Figure 2), there was a noticeable difference between the columns with and without added PG and lithium tracer. The real conductivity was constant (around 4mS/m) over time in the control columns filled with NaCl water. In the saturated part, the replicates showed the same behaviour for the real conductivity. For the contaminated columns a steady increase is noted in the first 21 days from 4mS/m to 8mS/m, and then a stabilisation for the remaining 10 days between 8 and 10mS/m was observed in all replicates.
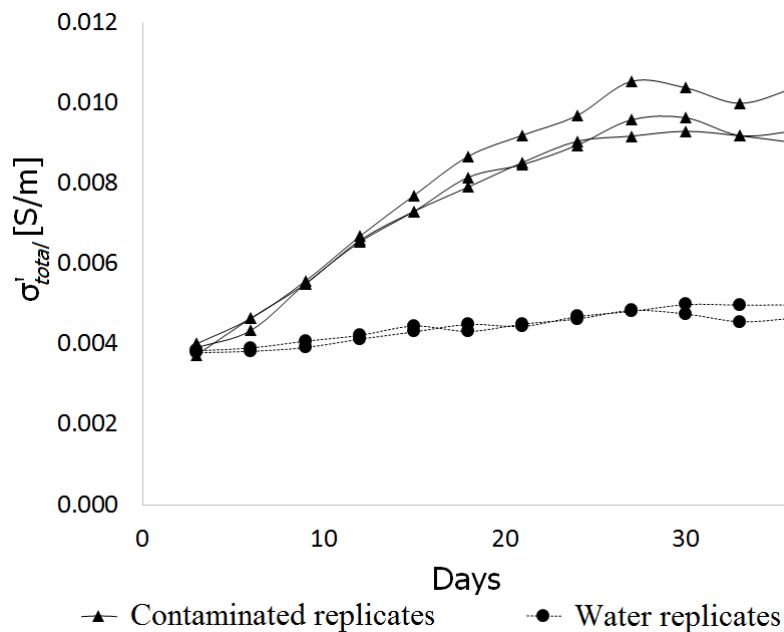

Figure 2. Bulk conductivity of the saturated zone in the contaminated columns (triangles) and in the control columns (circles).

In the unsaturated zone (Figure 3), measured between the potential electrode A and B, the difference between control and contaminated columns was noticeable too, although the measured conductivities were closer to each other (sometimes less than 2mS/m between a contaminated and a control replicate) than in the saturated zone. The variations between the replicates, both contaminated and control, were much higher, with often more 1-2mS/m of difference between the contaminated replicates, though the conductivity was always lower in the control than in the contaminated columns. In the upper unsaturated zone (Figure 3a), control

and contaminated columns were around 4mS/m on day 3, then the conductivity in the control columns remained constant, while it increased in the contaminated columns after day 10. In the lower unsaturated zone (Figure 3b), the conductivity started at around 10mS/m in the contaminated layer location, then decreased slightly over time in the contaminated columns. In the control columns, the real conductivity in the lower saturated zone (Figure 3b) was similar to the real conductivity in the upper saturated zone (Figure 3a).
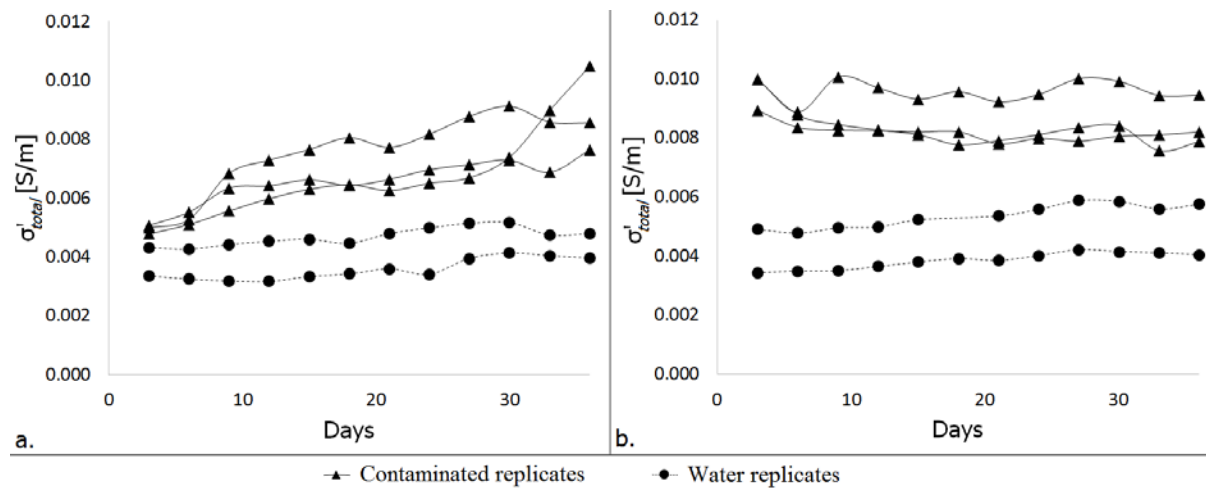

Figure 3. Bulk conductivity in the **a.** upper and **b.** lower unsaturated zone of the contaminated columns (triangles) and control columns (circles).

3.2. Imaginary conductivity

In the saturated zone, the imaginary conductivity (Figure 4) was different between the control and contaminated columns for low frequencies (between 0.01Hz and 1Hz). The imaginary conductivity increased in the contaminated column from day 3 to day 20 (0 to 50μS/m), then stabilised for the rest of the experiment. In contrast, the imaginary conductivity remained stable (around 0S/m) in the control columns. The polarisation was higher at 0.01Hz, but noisier. The trend is easier to observe at 0.1Hz and 1Hz even though the imaginary conductivity was lower. At 10Hz and higher, there were no significant difference between the control and contaminated columns.
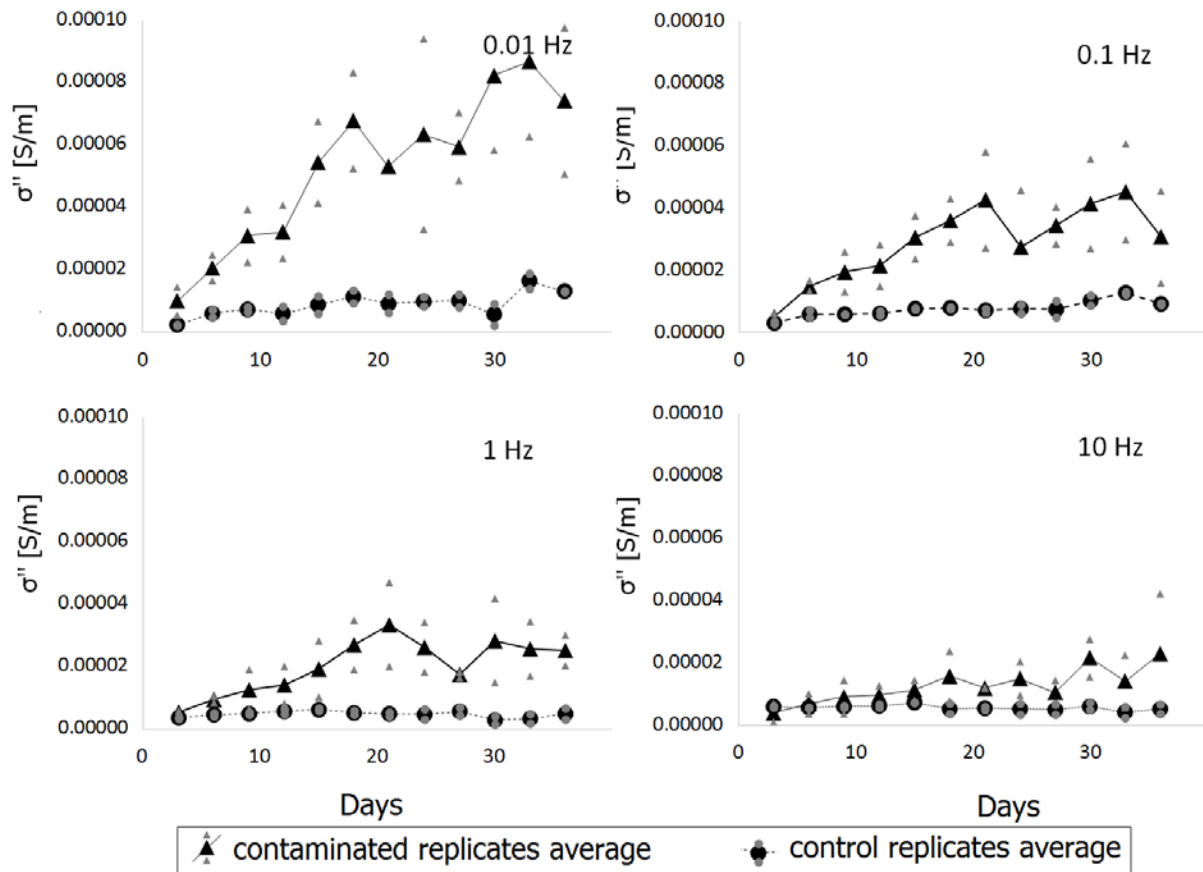
Figure 4. Imaginary conductivity in the saturated zone of the contaminated columns (triangles) and control columns (circles). Each curve shows the average $\pm$ one standard deviation (small symbols) between the replicates at the given frequencies (0.01, 0.1, 1 and 10Hz).

In the unsaturated zone, the imaginary conductivity was similar to the saturated zone, higher in the contaminated columns than in the control (Figure 5). The imaginary conductivity at 0.01Hz went from 40 to 80μS/m between day 3 to day 9, before stabilising around 60μS/m, while the control remained between 0 and 10μS/m throughout the experiment. However at 0.01Hz the deviation between the replicates is high. The trend is easier to observe at 0.1Hz, but at 1Hz and higher, there were no significant differences between the control and contaminated columns.
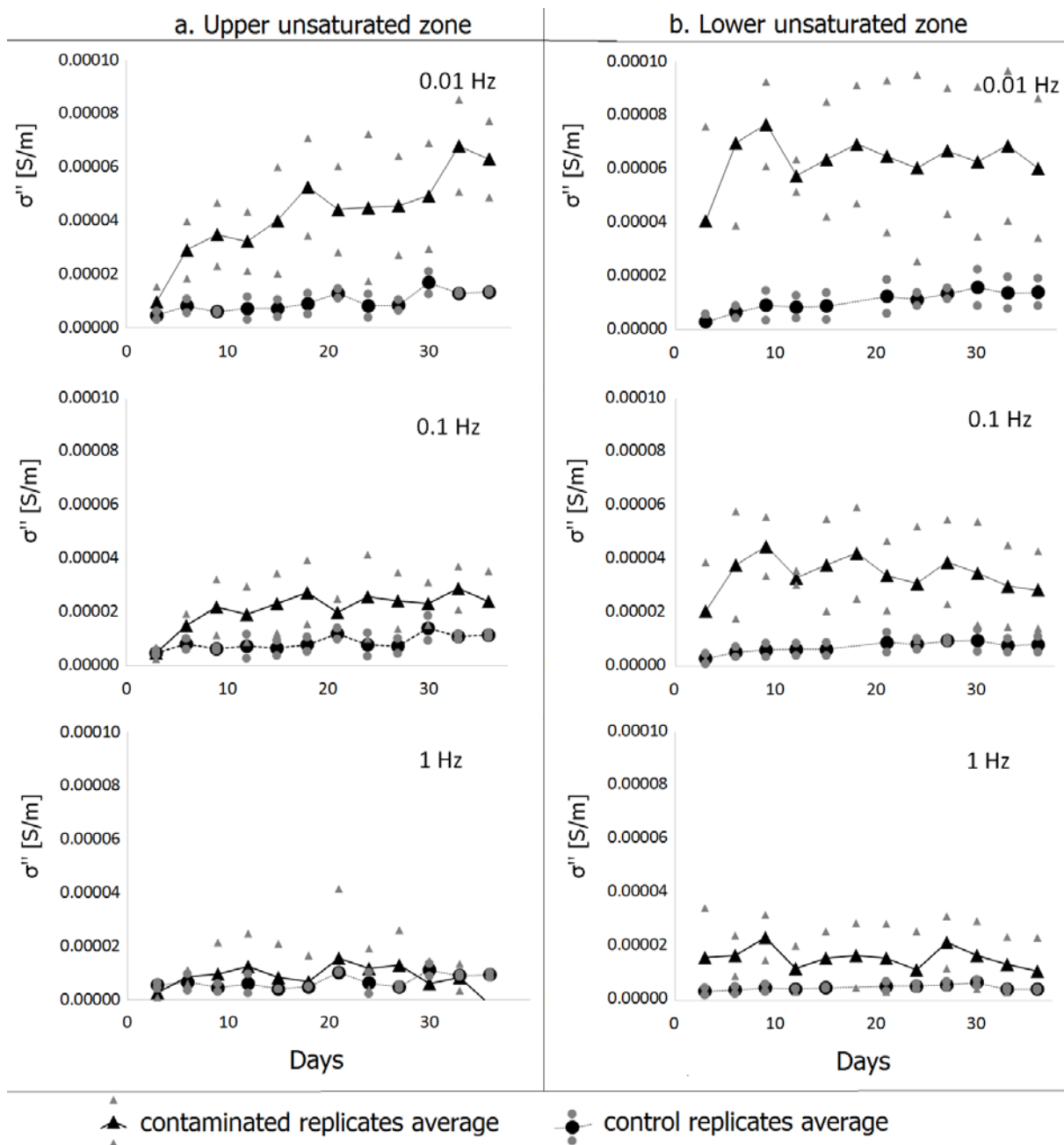
Figure 5. Imaginary conductivity of **a.** upper and **b.** lower unsaturated zone in the contaminated (triangles) and control columns (circles). Each curve shows the average $\pm$ one standard deviation (small symbols) between replicates at the given frequencies (0.01, 0.1 and 1Hz).

Outliers were removed for some replicates. In the lower unsaturated zone (Figure 5b), for the control columns (circles), all data collected on day 18 were removed for 0.01, 0.1 and 1Hz. In the saturated zone (Figure 4), of the contaminated columns (triangles) data for replicate 2 were removed from the average and standard deviation calculations for days 21 and 36 at 0.01Hz, and day 36 at 1Hz; replicate 3 was removed for days 21, 24 and 27 at 0.01Hz, day 27 at 1Hz and day 21 at 10Hz.

3.3. Pore-water samples

In the contaminated columns, increased iron and manganese concentrations in the pore water (Figure 6a) indicates that anaerobic conditions developed, this was also reflected in the increased real conductivity measurements (Figure 2).

In the unsaturated zone, the fluid electrical conductivity was high (650µS/cm) and remained stable throughout the experiment in the contaminated columns. It also remained stable in the control columns, but lower, similar to the NaCl solution added at the start of the experiment (250µS/cm) (Figure 6a). The pH (around 5) was stable over time in all the columns, and there was no significant differences between the control and contaminated columns (Figure 6b). The LiCl tracer and PG concentrations decreased over time (Figure 7) because both the lithium tracer and PG were diluted. A linear model (R^2=95%) could be fitted to the reduction in lithium tracer concentration over time, while PG reduction showed a poorer fit to a linear model (R^2=65%), hence other models of the reduction could fit equally well. Still, PG concentration seemed to decrease faster than the lithium tracer, which indicates that PG was degraded, and not only diluted.

PG degradation has a high oxygen demand, when oxygen is depleted, the next electron acceptor available in this soil is manganese oxide and then iron oxide. Hence, the development of anaerobic conditions in the columns can observed with the increased concentration of reduced manganese and iron in the pore water. In both contaminated and control columns, iron concentrations remained lower than 1mg/L (Figure 8a). In contrast, manganese concentration increased linearly by 2.6mg/L per day (R^2=93%) from 30mg/L on day 6 to 120mg/L on day 39 (Figure 8b) in the contaminated columns. Manganese concentrations in the control columns also increased from 6mg/L to 20mg/L during the first 10 days, after this, the concentration slowly doubled over the next 30 days. The increased manganese concentrations in the control columns indicate that some anaerobic degradation is occurring also here, which can be explained by the organic matter naturally present in the sand (1.8%). The presence of manganese in low concentration without contaminant in was also observed in a similar set up by Fernandez et al. (2018). The fact that manganese was observed both above and below the water table confirmed the presence of anaerobic pockets forming in the unsaturated zone, which saturation tend to 1 close to the water table.

In the saturated zone, the electrical conductivity remained the same as in the control column for the first 20 days. After this, the electrical conductivity in the contaminated columns

increased steadily, reaching more than 800µS/cm after 30 days, when the experiment ended (Figure 6a). The lithium tracer and PG concentrations remained low (<0.1mg/L), and were not measurable after 30 days. However, iron appeared in pore water of the contaminated columns (Figure 8a) after 18 days, going from 0.2mg/L on day 20 to 35mg/L on day 39. Manganese concentrations also started to increase significantly after 20 days, going from 40mg/L to 220mg/L when the experiment ended (Figure 8b).
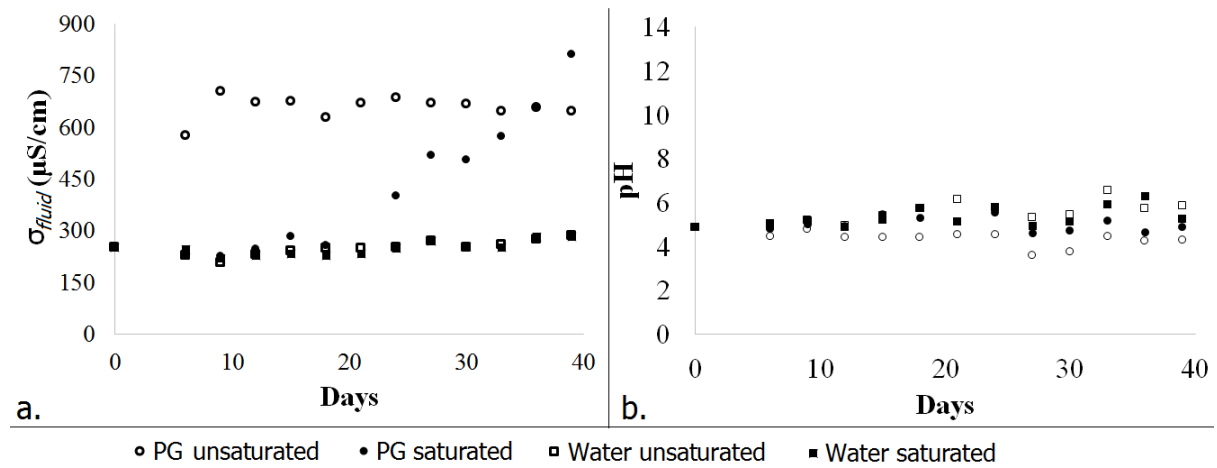

Figure 6. a. Electrical conductivity (σ_{fluid}) and **b.** pH in pore water samples for the water control columns and PG contaminated columns, both in unsaturated and saturated zones.
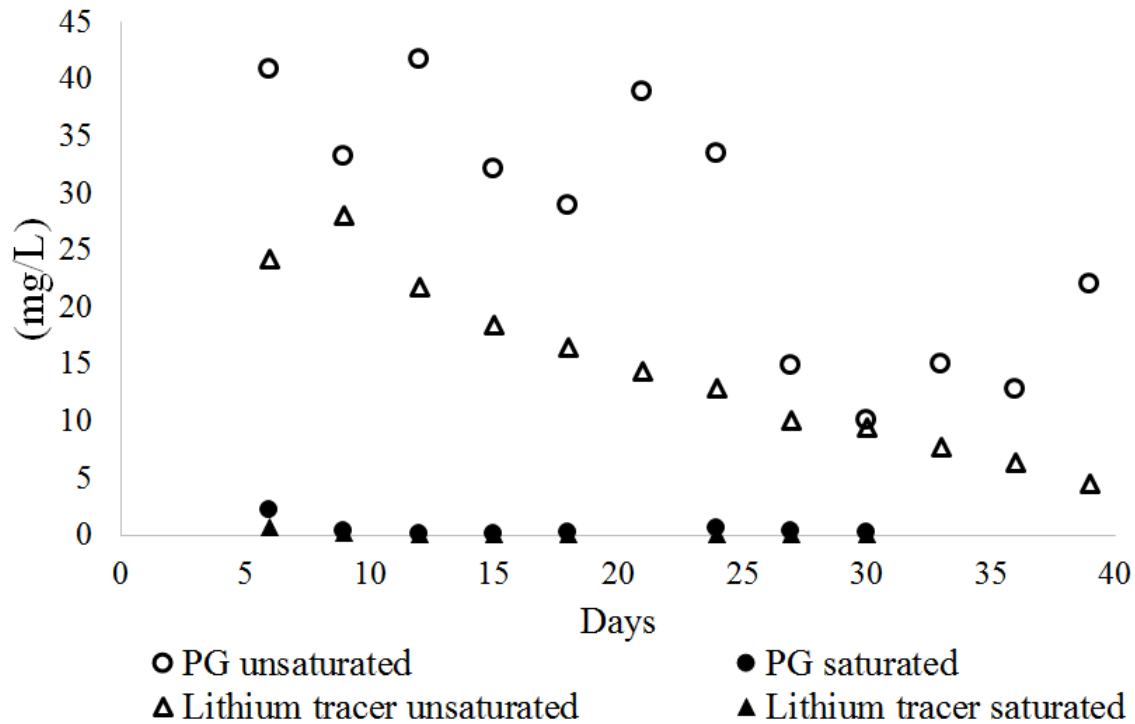

Figure 7. PG and lithium tracer evolution in the contaminated columns. After 30 days, the concentrations were under the detection limit in the saturated zone.
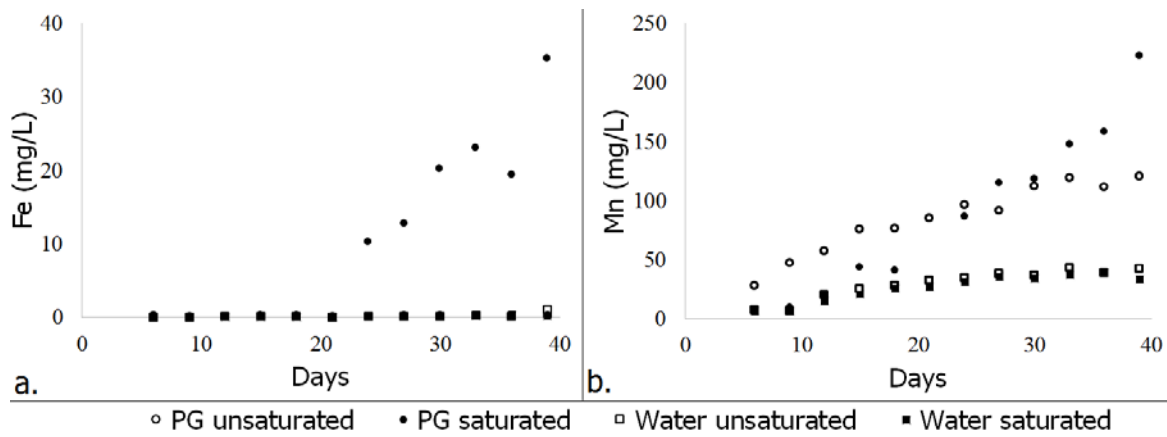
Figure 8. Concentrations of **a.** iron and **b.** manganese in the pore water samples in contaminated (PG) and control (water) columns.

3.4. Surface conductivity

In the saturated zone, the surface conductivity $\sigma'_{surface}$ was calculated from σ'_{total} (Figure 2) and σ_{fluid} (Figure 6a) using equation (2). Surface conductivity could be quantified in the contaminated columns (Figure 9a) but remained undetectable in the control columns (Figure 9b). In the contaminated columns, the σ_{fluid} contribution to the real conductivity remained constant around 4mS/m while the surface conductivity increased from nearly 0 to 4mS/m until day 18 (Figure 9a). Then the surface conductivity decreased to zero towards the end of the experiment, while σ_{fluid} tripled between day 18 and 36.
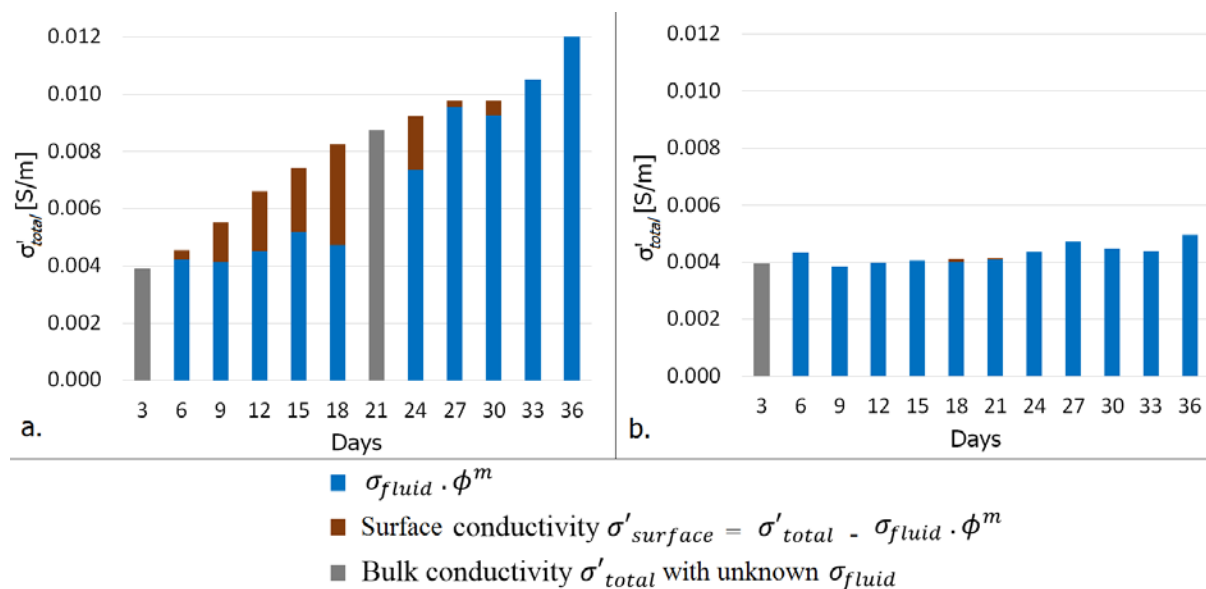

Figure 9. Bulk conductivity σ'_{total} expressed as the sum of the surface conductivity $\sigma'_{surface}$ (brown) and $\sigma_{fluid} \cdot \phi^m$ (blue) for **a.** the contaminated columns and **b.** the control columns. Grey bars indicate days with known bulk conductivity, but unknown σ_{fluid}.

4. Discussion

4.1. Development in the saturated zone

The results indicate that the experiment went through two stages of chemical processes in the saturated zone. The first stage starts from the first measurements (day 3 for SIP and day 6 for the water samples) until day 21. The second stage starts at day 21 to the last measurements (day 36 for SIP and day 39 for the water samples).

In the saturated zone, during stage 1, the complex conductivity, both real and imaginary, increased while the water electrical conductivity was constant, and no iron and low manganese were detected in the water samples. We suggest that amorphous primary iron oxide naturally present in the sand, such as ferric oxyhydroxides, were reduced to secondary iron oxides, such as semi conductive goethite, magnetite or hematite, which increased the bulk conductivity but not the pore water conductivity. Indeed, Lovley et al. (1987) describe anaerobic production of ultrafine-grained magnetite from amorphous ferric oxide during organic matter degradation. The conceptual model of Hansel et al. (2003) proposed that the metastable oxide ferrihydrite can form goethite and magnetite. The semi-conductive goethite has been observed with low Fe^{2+} concentration, as in the case of stage 1. Magnetite would be expected to form at higher Fe^{2+} concentration, however, ferrihydrite also sorbs Fe^{2+} and Fe^{2+} could, therefore, be underestimated in the water samples. More recently, Atekwana et al. (2014) suggested that increased conductivity in hydrocarbon contaminated site context could be explained by bio-mineral precipitation. They studied particularly the magnetic susceptibility within the zone of water table fluctuation at hydrocarbon-contaminated location. Mewafy et al. (2013) directly related magnetite concentration to increased imaginary conductivity between 1mHz and 10mHz, this is similar to the imaginary conductivity increase in our contaminated columns (Figure 4).

In the second stage, from day 21 to the end of the experiment on day 36, the secondary iron oxides were reduced as well, releasing Fe^{2+} (Figure 8a). Liu et al. (2011) showed that goethite can be reduced anaerobically to form Fe^{2+} and secondary minerals vivianite and dufrenite. The cation release increased the electrical conductivity of pore water (Figure 6a) from day 21, until the surface conductivity appeared negligible from day 30 (Figure 9). The constant and low lithium tracer concentration (Figure7) makes us confident that the increase in σ_{fluid} (Figure 6a) was mostly caused by iron and manganese release in pore water (Figure 8). As surface conductivity decreased at the same time that σ_{fluid} increased, the bulk conductivity

remained relatively stable. Also, the imaginary conductivity stayed fairly constant while the surface conductivity decreased (Figure 4), which is inconsistent with the conclusions of Weller et al. (2013), stating that the imaginary conductivity is positively correlated to the surface conductivity. Complementary explanations could account for this inconsistency. First, the porosity was most likely not constant, as assumed in the surface conductivity calculation, and the cementation factor could also be different to the assumed value of 1.3. Second, it is possible that what we assumed to be the surface conductivity is in fact a combination of the grain surface mineralogy and a biological factor, for example, growth of a conductive type of microorganism feeding on the carbon source (PG). Under anaerobic conditions, some bacteria have shown a conductive appendage, such as *Shewanella* (Gorby et al., 2006), *Geobacter* (Rabaey et al., 2007), and so-called cable bacteria (Pfeffer et al., 2012; Müller et al., 2016). This biomass growth would increase the surface conductivity but affect only marginally the imaginary conductivity, as discussed later. When PG was depleted, the microorganisms died and the biological part of the surface conductivity decreased (Figure 9). However, the imaginary conductivity linked to the grain surface mineralogy part of the surface conductivity remained constant (Figure 4).

In the absence of mineralogical and biological analysis, the explanation of the surface conductivity variations are purely hypothetical. However, the IP and chemical behaviour were the same in all replicates. The replicability of the results suggests that a similar experiment could be reproduced in order to add mineralogical investigations to test this hypothesis.

4.2. Development in the unsaturated zone

In the unsaturated zone, the real conductivity (Figure 3) depends on both the water content and chemistry. The water table was fixed at the same level in all the columns, but local heterogeneities could have caused differences in the capillary fringe, which would explain the differences between the replicates. Because of the heterogeneous saturation in the unsaturated zone, it was not possible to estimate the proportion of the real conductivity explained by the surface conductivity. Still, the water chemistry was a significant contributor to the real conductivity because the contaminated samples were more conductive than the controls. Moreover, the contribution from the water conductivity must have been relatively constant, as deduced from electrical conductivity of the water samples (Figure 6a). The imaginary conductivity also allows us to distinguish two stages of the experiment, the first 10 days when the imaginary conductivity increased in the contaminated columns, and the rest of the

experiment where it remained stable. The mechanisms driving the imaginary conductivity response were observed at an even lower frequency range than in the saturated zone, as the difference between control and contaminated columns was only noticeable up to 0.1Hz in the unsaturated zone (Figure 5). Multiple explanations could account for this behaviour. The bacterial growth could have been more important, due to the oxygen initially present in the air-filled pores. Iron concentrations were very low (Figure 8a), but as discussed before, it is compatible with goethite formation. Moreover, manganese dioxide was used as electron acceptor, as confirmed by Mn^{2+} concentrations measured in the pore water (Figure 8b), so the more conductive manganese oxide (MnO) could have formed.

Observations of manganese in the pore water both in the saturated and unsaturated zone (Figure 8b) proved that anaerobic conditions developed also above the water table. Similarly, the imaginary conductivity increased at 0.1Hz both above the water table (Figure 5) and in the saturated zone (Figure 4), even though the signal was not as clear. Even though anaerobic conditions developed above the water table, more oxygen was most likely available and therefore only manganese oxides were reduced.

4.3. Influence of biomass growth on the results

Microorganisms are responsible for degradation of organic compounds (e.g. Huntera et al., 1998; Rabaey et al., 2007) and degradation is clearly indicated from the release of manganese and iron measured in the water samples (Figure 8). Multiple studies showed that bacterial growth tends to increase the complex conductivity of the soil. For example, Abdel Aal et al. (2004) compared biotic and abiotic complex conductivity of an organic compound contaminant (diesel) in a laboratory saturated sand column experiment. They showed that in the presence of a bacterial community, the contaminated sand complex conductivity increased over time, and that such a change was not observed in strictly abiotic conditions. Abdel Aal et al. (2006) also investigated sediment samples from a site contaminated by hydrocarbon undergoing intrinsic biodegradation and deduced that the accumulation of microbial cells and biofilm with high surface area at the mineral-electrolyte interface generates the IP response. More recently, Revil et al. (2012) developed a model describing the complex conductivity during bacterial growth in a porous material. The model shows that the imaginary conductivity increases (or decreases) linearly with the density of bacteria cells given that the bacteria concentration remains a dilute solution. Based on these experiences, Revil et al. (2012) and Abdel Aal et al. (2010) suggest IP as a suitable method for monitoring biodegradation of organic compounds. However, as discussed by Williams et al (2009) for a similar result, the

phase increase due to bacterial growth alone (about 1mrad) is an order of magnitude lower than the mineral formation they caused (about 10mrad) (e.g. Williams et al., 2005, Ntarlagiannis et al., 2005). Moreover, the carbon-based contaminant investigated in this study is an antibacterial (Nalawade et al., 2015; Olitzky, 1965). As discussed earlier in the developments in the saturated zone, the bacterial community might play an important part in the calculated surface conductivity (Figure 9), but influence the imaginary conductivity (Figure 4 and 5) in relatively low proportion. As for the mineralogy, a microbiological investigation should be conducted in a replication of the presented experiment to understand the part played by microorganisms in the chemical processes and the influence of their development on the SIP signal.

4.4. Assumptions of water chemistry and porosity

Water chemistry: Despite anaerobic conditions that allowed manganese release (Figure 8b), iron concentrations remained low. Three possible reasons could explain this, each not incompatible with each other. First, the iron oxides were not yet accepted as an electron acceptor. Second, Fe^{2+} produced within an anaerobic pocket could be re-oxidised immediately with arrival of dissolved oxygen coming from still aerobic pockets. Finally, iron concentrations measured in the water samples are an underestimation of the pore water iron concentration because the sampling, even though quick, was done aerobically and that iron precipitation is almost immediate in contact with oxygen. Although, significant concentrations of iron were measured later in the saturated zone, validating the sampling technique to some extent, the sampling effect could also explain why the iron concentration are lower than those observed in similar environments (e.g. Fernandez et al., 2018; Williams et al., 2009).

Porosity: To calculate the surface conductivity in the saturated zone, the porosity was assumed constant in all columns, which is unlikely. However, if the porosity was changing of ±10%, which is more than the deviation between the test (less than 5%), the surface conductivity would still be observed in the contaminated columns, as shown in Table 1.

Table 1. Sensitivity of the surface conductivity to porosity variations.

	-10%	**measured**	**+10%**
Porosity	0.369	0.41	0.451
Average surface conductivity in the contaminated columns	2.11mS/m	1.22mS/m	0.25mS/m
Occurring period in the contaminated columns	From day 6 to day 33	From day 6 to day 30	From day 9 to day 24

5. Conclusion

The study emphasised both the difficulty and the great necessity to produce replicable results, which quantify differences caused by natural variability rather than treatment. The interpretation of such results are consequently more difficult, but also more reliable. For all replicas, the anaerobic reduction of iron and manganese oxide during the organic degradation increased both the conductive and polarisation component of the complex conductivity.

The development of reducing condition at the water table interface caused by degradation of an organic contamination increases the complex conductivity. The real conductivity calculated from SIP measurements was sensitive to iron and manganese dissolution caused by anaerobic degradation, as expected. The comparison between the bulk real conductivity and pore water conductivity highlighted the formation of a semi-conductive mineral preceding the release of iron cations in the saturated zone. The imaginary conductivity at low frequencies was also sensitive to the degradation, both in the saturated and unsaturated zones. The use of 0.1Hz frequency seems to be the best compromise to identify imaginary conductivity changes due to the organic degradation, while only suffering few outliers. The increase in imaginary conductivity in the saturated zone preceded the iron release in pore water.

Hence, SIP could possibly be an appropriate method to indicate when iron oxides start to be used as electron acceptor before iron is released in pore water. However, this hypothesis could only be confirmed by linking the SIP measurements to a time-lapse mineralogy analysis. Conducting time lapse mineralogy analysis in parallel of the water samples using a similar setup would help us to better understand the changes in solid (mineralogical) chemistry that precede the ions release caused by the anaerobic degradation. Including microbial analysis (cell counts, DNA) makes it possible to understand the evolution of the general microbial population as well as the part of aerobic and anaerobic microorganisms through the length of the experiment.

References

Abdel Aal, G., Atekwana, E., Rossbach, S. and Werkema, D. (2010). Sensitivity of geoelectrical measurements to the presence of bacteria in porous media. Journal of Geophysical Research, 115, G03017.

Abdel Aal, G., Atekwana, E., Slater, L. and Atekwana, E. (2004). Effects of microbial processes on electrolytic and interfacial electrical properties of unconsolidated sediments. Geophysical Research Letters, 31(12), L12505.

Abdel Aal, G., Slater, L. and Atekwana, E. (2006). Induced-polarisation measurements on unconsolidated sediments from a site of active hydrocarbon biodegradation. *GEOPHYSICS*, 71(2), pp.H13-H24.

Appelo, C. and Postma, D. (2010). Geochemistry, Groundwater and Pollution, Second Edition, pp. 440.

Arora, T., Linde, N., Revil, A. and Castermant, J. (2007). Non-intrusive characterization of the redox potential of landfill leachate plumes from self-potential data. *Journal of Contaminant Hydrology*, 92(3-4), pp.274-292.

Atekwana, E., Mewafy, F., Abdel Aal, G., Werkema, D., Revil, A. and Slater, L. (2014). High-resolution magnetic susceptibility measurements for investigating magnetic mineral formation during microbial mediated iron reduction. *Journal of Geophysical Research: Biogeosciences*, 119(1), pp.80-94.

Balbarini, N., Rønde, V., Maurya, P., Fiandaca, G., Møller, I., Erik Klint, K., Christiansen, A., Binning, P. and Bjerg, P. (2018). Geophysics Based Contaminant Mass Discharge Quantification Downgradient of a Landfill and a Former Pharmaceutical Factory. *Water Resources Research*, 54 (8), pp. 5436-5456

Carlson, N., Bouzid, N. and Byrd, R. (2015). Environmental applications of the IP method: Surveys of subsurface waste. *The Leading Edge*, 34(2), pp.214-220.

Fernandez, P.M., Bloem, E. and French, H. (2015). Redox measurements; A commercial combined probe method versus the half-cell multiple distance probes method. Poster, Freudenstadt workshop.

Fernandez, P.M., Bloem, E., Binley, A., Philippe, R. and French, H. (2018). Monitoring redox sensitive conditions at the groundwater interface using electrical resistivity and self-potential. Manuscript. Submitted to Journal of Contaminant Hydrology

French, H.K. and Binley, A. (2004). Snowmelt infiltration: monitoring temporal and spatial variability using time-lapse electrical resistivity. *Journal of Hydrology*, 297(1-4), pp.174-186.

French, H.K., Van der Zee, S.E.A.T.M. and Leijnse, A. (1999) Differences in gravity dominated unsaturated flow during autumn rains and snowmelt. *Hydrological processes*, 13, 17: 2783-2800

French, H.K., Van der Zee, S. and Leijnse, A. (2001). Transport and degradation of propyleneglycol and potassium acetate in the unsaturated zone. *Journal of Contaminant Hydrology*, 49(1-2), pp.23-48.

Gorby, Y., Yanina, S., McLean, J., Rosso, K., Moyles, D., Dohnalkova, A., Beveridge, T., Chang, I., Kim, B., Kim, K., Culley, D., Reed, S., Romine, M., Saffarini, D., Hill, E., Shi, L., Elias, D., Kennedy, D., Pinchuk, G., Watanabe, K., Ishii, S., Logan, B., Nealson, K. and Fredrickson, J. (2006). Electrically conductive bacterial nanowires produced by Shewanella oneidensis strain MR-1 and other microorganisms. *Proceedings of the National Academy of Sciences*, 103(30), pp.11358-11363.

Hansel, C., Benner, S., Neiss, J., Dohnalkova, A., Kukkadapu, R. and Fendorf, S. (2003). Secondary mineralization pathways induced by dissimilatory iron reduction of ferrihydrite under advective flow. *Geochimica et Cosmochimica Acta*, 67(16), pp.2977-2992.

Huntera, K., Wang, Y. and Van Cappellena, P. (1998). Kinetic modeling of microbially-driven redox chemistry of subsurface environments: coupling transport, microbial metabolism and geochemistry. *Journal of Hydrology*, 209(1-4), pp.53-80.

Jaesche, P., Totsche, K. and Kögel-Knabner, I. (2006). Transport and anaerobic biodegradation of propylene glycol in gravel-rich soil materials. *Journal of Contaminant Hydrology*, 85(3-4), pp.271-286.

Kemna, A., Binley, A. and Slater, L. (2004). Crosshole IP imaging for engineering and environmental applications. *GEOPHYSICS*, 69(1), pp.97-107.

Lindberg, R. and Runnells, D. (1984). Ground Water Redox Reactions: An Analysis of Equilibrium State Applied to Eh Measurements and Geochemical Modeling. *Science*, 225(4665), pp.925-927.

Lissner, H., Wehrer, M., Jartun, M. and Totsche, K. (2013). Degradation of deicing chemicals affects the natural redox system in airfield soils. Environmental Science and Pollution Research, 21(15), pp.9036-9053.

Liu, D., Wang, H., Dong, H., Qiu, X., Dong, X. and Cravotta, C. (2011). Mineral transformations associated with goethite reduction by Methanosarcina barkeri. *Chemical Geology*, 288(1-2), pp.53-60.

Lovley, D., Stolz, J., Nord, G. and Phillips, E. (1987). Anaerobic production of magnetite by a dissimilatory iron-reducing microorganism. *Nature*, 330(6145), pp.252-254.

Martens, V. V., Amundsen, C.-E. and Bergersen, O. (2012). Research on Conservation State and Preservation Conditions in Unsaturated Archaeological Deposits in Oslo. *Conservation and Management of Archaeological Sites*, 14(1-4), pp.72-84.

Maurya, P., Rønde, V., Fiandaca, G., Balbarini, N., Auken, E., Bjerg, P. and Christiansen, A. (2017). Detailed landfill leachate plume mapping using 2D and 3D electrical resistivity tomography - with correlation to ionic strength measured in screens. *Journal of Applied Geophysics*, 138, pp.1-8.

Mewafy, F., Werkema, D., Atekwana, E., Slater, L., Abdel Aal, G., Revil, A. and Ntarlagiannis, D. (2013). Evidence that bio-metallic mineral precipitation enhances the complex conductivity response at a hydrocarbon contaminated site. *Journal of Applied Geophysics*, 98, pp.113-123.

Müller, H., Bosch, J., Griebler, C., Damgaard, L., Nielsen, L., Lueders, T. and Meckenstock, R. (2016). Long-distance electron transfer by cable bacteria in aquifer sediments. *The ISME Journal*, 10(8), pp.2010-2019.

Murphy, C., Wallace, S., Knight, R., Cooper, D. and Sellers, T. (2015). Treatment performance of an aerated constructed wetland treating glycol from de-icing operations at a UK airport. *Ecological Engineering*, 80, pp.117-124

Nalawade, T., Sogi, S. and Bhat, K. (2015). Bactericidal activity of propylene glycol, glycerine, polyethylene glycol 400, and polyethylene glycol 1000 against selected microorganisms. *Journal of International Society of Preventive and Community Dentistry*, 5(2), p.114.

Nitschke, L., Wagner, H., Metzner, G., Wilk, A. and Huber, L. (1996). Biological treatment of waste water containing glycols from de-icing agents. *Water Research*, 30(3), pp.644-648.

Ntarlagiannis, D., Yee, N. and Slater, L. (2005). On the low-frequency electrical polarization of bacterial cells in sands. *Geophysical Research Letters*, 32(24), L24402.

Nyquist, J. and Corry, C. (2002). Self-potential: The ugly duckling of environmental geophysics. The Leading Edge, 21(5), pp.446-451.

Olitzky, I. (1965). Antimicrobial Properties of a Propylene Glycol Based Topical Therapeutic Agent. *Journal of Pharmaceutical Sciences*, 54(5), pp.787-788.

Placencia-Gómez, E., Slater, L., Ntarlagiannis, D. and Binley, A. (2013). Laboratory SIP signatures associated with oxidation of disseminated metal sulfides. *Journal of Contaminant Hydrology*, 148, pp.25-38.

Petersén, A. and Bergersen, O. (2012). An Assessment of the Status and Condition of Archaeological remains Preserved In Situ in the Medieval Town of Trondheim Based on Archeochemical Investigations conducted During the Period 2007-2010*, Conservation and management of archaeological sites*, 14(1–4), pp72-84 and 228–38.

Petersén, A. and Bergersen, O. (2016). The In Situ Preservation in the Unsaturated Zone: Results from Environmental Investigations at the 'Schultz Gate' Case Study in the Medieval Town of Trondheim, Norway. *Conservation and Management of Archaeological Sites*, 18(1-3), pp.181-204.

Pfeffer, C., Larsen, S., Song, J., Dong, M., Besenbacher, F., Meyer, R., Kjeldsen, K., Schreiber, L., Gorby, Y., El-Naggar, M., Leung, K., Schramm, A., Risgaard-Petersen, N. and Nielsen, L. (2012). Filamentous bacteria transport electrons over centimetre distances. *Nature*, 491(7423), pp.218-221.

Rabaey, K., Rodríguez, J., Blackall, L., Keller, J., Gross, P., Batstone, D., Verstraete, W. and Nealson, K. (2007). Microbial ecology meets electrochemistry: electricity-driven and driving communities. *The ISME Journal*, 1(1), pp.9-18.

Revil, A., Atekwana, E., Zhang, C., Jardani, A. and Smith, S. (2012). A new model for the spectral induced polarisation signature of bacterial growth in porous media. *Water Resources Research*, 48(9), W09545.

Schlumberger, C. (1920). *Étude sur la prospection électrique du sous-sol.* Paris: Gauthier-Villars.

Slater, L., Choi, J. and Wu, Y. (2005). Electrical properties of iron-sand columns: Implications for induced polarisation investigation and performance monitoring of iron-wall barriers. *GEOPHYSICS*, 70(4), pp.G87-G94.

Søiland, A. (2011) Geophysical monitoring of degradable de-icing chemicals in the saturated zone during snowmelt. Master Thesis. Ås. Norwegian University of Life Sciences. p.33

Weller, A., Slater, L. and Nordsiek, S. (2013). On the relationship between induced polarization and surface conductivity: Implications for petrophysical interpretation of electrical measurements. *GEOPHYSICS*, 78(5), pp.D315-D325.

Williams, K., Kemna, A., Wilkins, M., Druhan, J., Arntzen, E., N'Guessan, A., Long, P., Hubbard, S. and Banfield, J. (2009). Geophysical Monitoring of Coupled Microbial and Geochemical Processes During Stimulated Subsurface Bioremediation. *Environmental Science & Technology*, 43(17), pp.6717-6723.

Williams, K., Ntarlagiannis, D., Slater, L., Dohnalkova, A., Hubbard, S. and Banfield, J. (2005). Geophysical Imaging of Stimulated Microbial Biomineralization. *Environmental Science & Technology*, 39(19), pp.7592-7600.